Water entry of spheres at various contact angles

Nathan B. Speirs[1], Mohammad Mansoor[1], Jesse Belden[2] and Tadd T. Truscott[1]†

[1]Department of Mechanical and Aerospace Engineering, Utah State University, Logan, UT 84322, USA

[2]Naval Undersea Warfare Center Division Newport, 1176 Howell Street, Newport, Rhode Island 02841, USA.

(Received xx; revised xx; accepted xx)

It is well known that the water entry of a sphere causes cavity formation above a critical impact velocity as a function of the solid-liquid contact angle (Duez *et al.* 2007). Using a rough sphere with a contact angle of 120°, Aristoff & Bush (2009) showed that there are four different cavity shapes dependent on the Bond and Weber numbers (i.e., quasi-static, shallow, deep and surface). We experimentally alter the Bond number, Weber number and contact angle of smooth spheres and find two key additions to the literature: 1) Cavity shape also depends on the contact angle; 2) the absence of a splash crown at low Weber number results in cavity formation below the predicted critical velocity. In addition, we find an alternate scaling for the Bond and Weber numbers that predicts cavity shapes for various impacting bodies (e.g., spheres, multi-droplet streams and jets) on the same regime diagram, thus, merging the often separated studies of solid-liquid and liquid-liquid impact in the literature.

1. Introduction

At the turn of the millennium a resurgence of interest occurred in water entry studies. During this time, two foundational papers on cavity formation and cavity dynamics were published, which describe the regimes into which all other water entry studies fall. The first was written by Duez *et al.* (2007) who investigated when impacting spheres form air cavities, as shown in figure 1b-e, and when they do not, as shown in figure 1a. The second paper, written by Aristoff & Bush (2009), came along a couple of years later discussing the four different shapes or types of cavities that form once the appropriate conditions are met for cavity formation (shown in figure 1b-e). We will now examine each of these papers in turn, discussing their findings, an unaddressed discrepancy between the two, and how this paper expands our understanding of the conditions in which these five water entry regimes occur.

Duez *et al.* (2007) found that cavity formation of smooth spheres occurs above a critical velocity U_{cr} that is a function of the advancing static contact angle θ. Hydrophilic spheres ($\theta < 90°$) form cavities above $U_{cr} \approx 7.2$ m/s in water. The critical velocity decreases for hydrophobic spheres ($\theta > 90°$) going to zero as θ goes to 180°. They explain this finding by discussing the contact-line stability of the thin, upward-moving film or splash that forms around the circumference of the sphere upon impact. When the splash adheres to the sphere (below the critical velocity) no cavity forms. When it separates from the sphere, air gets pulled behind the sphere and a cavity forms.

† Email address for correspondence: taddtruscott@gmail.com

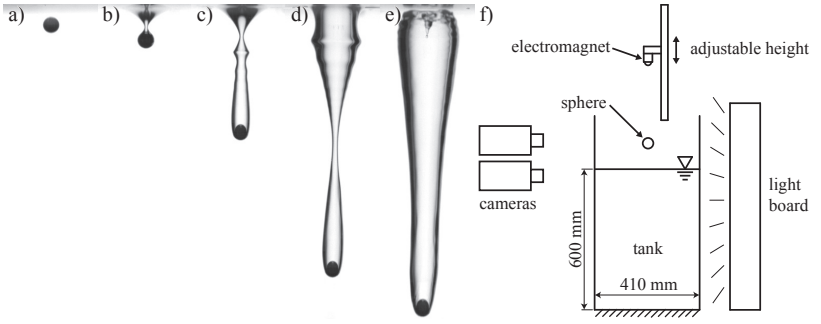

FIGURE 1. A 2 mm diameter sphere impacts the water surface creating various cavity types. In a) the wetting angle is $\theta = 101.0^\circ$ and the sphere impacts at 4.43 m/s without forming a cavity. In b) through e) the sphere has a wetting angle of $\theta = 141.1^\circ$ and impacts with velocities 0.24 m/s, 1.40 m/s, 2.80 m/s, and 4.43 m/s forming quasi-static, shallow, deep, and surface seal cavities, respectively. See supplementary movies 1-5. f) The basic experimental setup is shown with two high-speed camera viewing the impact events above and below the free surface.

Aristoff & Bush (2009) studied the water entry of spheres with one contact angle, $\theta = 120 \pm 5^\circ$, and various impact velocities and sphere diameters. Their expansive data set found cavities forming at all impact velocities with four distinct shapes defined by their collapse or pinch-off location, each of which occurs at a specific location on a Bond-Weber plot. At the lowest Weber number, We, they describe quasi-static seal, in which pinch-off occurs on or very near the sphere surface (figure 1b). At higher We both shallow and deep seal are seen. Shallow seal occurs at lower Bond number, Bo, where surface tension dominates and the pinch-off depth is on the order of the capillary length (figure 1c). Deep seal occurs at higher Bo, where gravitational forces dominate and pinch-off occurs about half way between the pool surface and the sphere (figure 1d). Surface seal occurs at the highest We, wherein the splash created upon impact collapses inward due to air pressure and surface tension (Marston *et al.* 2016) sealing at the pool surface (figure 1e).

According to Duez *et al.* (2007), at the contact angle used by Aristoff & Bush (2009) ($\theta = 120^\circ$), cavities should not form below $U_{cr} = 2.14$ m/s. Yet Aristoff & Bush report quasi-static, shallow and deep seal cavities at velocities below this value. We can explain this discrepancy by the high surface roughness of the coating used by Aristoff & Bush, Cytonix WX2100, which, in our own testing we have found to have a large ten-point-mean roughness of $R_z = 50.2 \pm 21.4$ μm. Zhao *et al.* (2014) found that U_{cr} is also a function of the sphere roughness R_z, with increasing roughness leading to lower values of U_{cr}. Cavities should always form at the above value of R_z and hence the cavity formation described in work of Aristoff & Bush (2009) is due to both the high contact angle and high roughness.

Since these foundational works, several other important studies have come forth. Important topics include: the water entry of spinning spheres (Truscott & Techet 2009*a*,*b*), the effect of sphere density (Aristoff *et al.* 2010), the occurrence of multiple pinch-off events (Mansoor *et al.* 2014), the buckling instability in the crown (Marston *et al.* 2016), the effects of deformability (Hurd *et al.* 2017), the unsteady forces during entry (Truscott *et al.* 2012), and many more described in the annual review by Truscott *et al.* (2014).

Although these works have contributed much to our understanding of water entry, we will return our focus to the foundational works discussed above and examine how the cavity formation regimes respond to experimentally varying the wetting angle θ, the sphere diameter d and the impact velocity U_o for smooth spheres. We will explain the

Coating	θ	R_z (μm)
Clean Steel	$86.1 \pm 2.2^\circ$	0.6 ± 0.3
Turtle Wax Super Hard Shell	$101.0 \pm 4.7^\circ$	0.9 ± 0.2
Cytonix WX2100	$116.6 \pm 7.0^\circ$	50.2 ± 21.4
Glaco Mirror Coat Zero	$141.1 \pm 3.8^\circ$	1.0 ± 0.5

TABLE 1. List of coatings with their advancing static contact angle θ and ten point mean roughness R_z, with the mean and 95% confidence window reported.

physics using the Bond, Weber, and Froude numbers, which we define as $Bo = \rho g d^2/\sigma$, $We = \rho U_o^2 d/\sigma$ and $Fr = U_o^2/gd$, respectively, where ρ is the liquid density, g is the acceleration of gravity and σ is the surface tension. We use the diameter d instead of the sphere radius as the appropriate length scale in defining the above dimensionless numbers as it results in transitional behaviors around a value of one. In § 4 we will also examine an alternate method of defining the Bond, Weber, and Froude numbers that allows us to predict the cavity types for various impacting bodies on the same regime diagram.

2. Experimental setup and description

Figure 1f shows the experimental setup used in this study. Various diameter stainless steel spheres ($d_s = 1$ to 18 mm) of specific gravity 7.83 are dropped from an electromagnet onto a tank of water. Two high-speed cameras record the impact on the free-surface, imaging at 2,500 frames per second both above and below the surface from the side. The height of the electromagnet controls the impact velocity of the spheres U_o, which is varied from 0.24 to 10.39 m/s. To vary the advancing static contact angle θ three different coatings (or the lack thereof) are used: clean steel, Turtle Wax Super Hard Shell car wax, and Glaco Mirror Coat Zero. Values of θ and the ten point mean roughness R_z are shown in table 1. Roughness measurements are obtained using a profilometer. The spheres are prepared by first washing with soap and water and then rinsing with ethyl alcohol. Coatings are then applied and allowed to dry before testing. After each test the spheres are dried and then recoated to ensure consistent surface properties.

From the high-speed videos we determine whether or not a cavity forms. If a cavity does form, the cavity type is determined using the definitions described by Aristoff & Bush (2009). Measurements are also taken from the videos to find cavity depths, diameters, and the time to pinch-off. The pinch-off depth h_p is defined as the distance from the undisturbed free surface to the location where the cavity walls or splash pinch together or collapse (positive downward). The depth of the bottom of the sphere at the time of pinch-off, h_b, is also measured from the undisturbed free surface. The pinch-off time t_p is defined as the time from impact to the pinch-off event. In cases where cavities do not form, we define the pinch-off time t_p as the time when the splash closes on the top of the sphere and the pinch-off depth h_p as the location of the top of the sphere at this time. The cavity diameter is measured at discrete depths and times and the maximum cavity diameter over time is found at discrete depths, yielding $d_{c,max}(z)$. The average of these maximum diameters over all depths defines d_c.

3. Cavity formation and types

Multiple sphere diameters were tested over a large range of impact velocities for each contact angle. From these data we produce Bo-We plots similar to Aristoff & Bush

(2009) to examine how the cavity regimes change with the contact angle (figure 2). The regime diagram for $\theta = 86.1°$ is shown in figure 2a. Duez *et al.* (2007) predict the critical velocity for cavity formation for a hydrophilic sphere to be $U_{cr} = 0.1\sigma/\mu = 7.2$ m/s, which is represented by the dashed line in figure 2a. Surface seal cavities occur above this dashed line (as shown in figure 1e) and no cavity formation is observed just below it (figure 1a). Once We has decreased below about 240, cavities start to form again, which is unexpected in light of the work of Duez *et al.* (2007). Below $We \approx 240$ spheres always form quasi-static seal cavities.

Looking at the regime diagram for $\theta = 101.0°$ (figure 2b) we see a similar trend to $\theta = 86.1°$ with a few differences. The critical velocity for cavity formation as predicted by Duez et al. has decreased due to the increased contact angle and is defined by $U_{cr} = \frac{7}{270}\frac{\sigma}{\mu}(\pi - \theta)^3 = 4.89$ m/s. The critical We below which cavities form again does not changed with the increase in θ. Below $We \approx 240$ mostly quasi-static seal cavities form with the exception of a few shallow seal cavities at low Bo, for which the volume of air entrained with the sphere is small, but approximately equal to the volume of the sphere (this is consistent with the cut-off defined by Aristoff & Bush (2009)).

To understand why cavities form below a $We \approx 240$ we look at what happens as the velocity or We increases for a given sphere diameter or Bo. Figure 3a shows the impact of a 10 mm diameter sphere at various We when the sphere is approximately half submerged. At the lowest We a short, thick rim forms around the edge of the sphere. This rim does not have enough upward velocity to climb up the surface of the sphere and meet itself at the pole to prevent cavity formation (Duez *et al.* 2007). Hence, as the sphere descends, the free-surface is pulled down with the sphere and a quasi-static seal cavity forms in its wake (figure 3b & c, $We = 7.9$). As We increases the rim thins and grows taller due to its increasing upward velocity, which allows it to begin to climb the surface of the sphere as seen in figure 3a at $We = 109$. The upward velocity and adherence of the rim to the sphere directly competes with the rate of sphere submergence. This causes the water to move up and around the top of the sphere faster as it descends below the original free-surface plane, resulting in less air entrainment and the formation of increasingly smaller cavities. Hence, the pinch-off time t_p, depth of the sphere at pinch-off h_b, and the pinch-off depth h_p, all decrease with increasing We which can be seen qualitatively in figure 3 and quantitatively in figure 4. Once $We > \approx 240$ (dotted line) the rim has formed into a splash which has enough upward velocity to reach the top of the sphere by the time the top of the sphere has descended to the level of the undisturbed free-surface ($h_p = 0$ and $h_b = 1$, figure 4b & c), as seen at $We = 269$ in figure 3b & c. Hence, the formation of the splash (which adheres to the sphere) suppresses cavity formation and we will call the dotted lines in figures 2a & b and 3 the *splash formation line*.

As We increases above the *splash formation* line the splash climbs up the sphere surface faster causing h_p to gradually rise above the free-surface (figure 4c), and decreasing both t_p (figure 4a) and h_b (figure 4b). Around U_{cr}, a small asymmetric cavity forms with the splash quickly doming over the top (figure 3, $We = 2696$). Once U_{cr} is reached, the splash has enough velocity to separate from the sphere and a large surface seal cavity forms (figure 3, $We = 8081$). Hence, we see that cavity formation or suppression is governed by the formation and separation of the splash. Also, we find that cavity formation occurs in two regimes: at low enough We that a splash does not form, and at high enough impact velocity that the splash separates from the sphere. The boundaries of the no cavity regime are defined by *splash formation* and what we will call *Duez cavity formation* (dotted and dashed lines in figure 2a & b and 3, respectively).

Surface seal is caused by the collapse of the splash crown. In the ideal cases typically

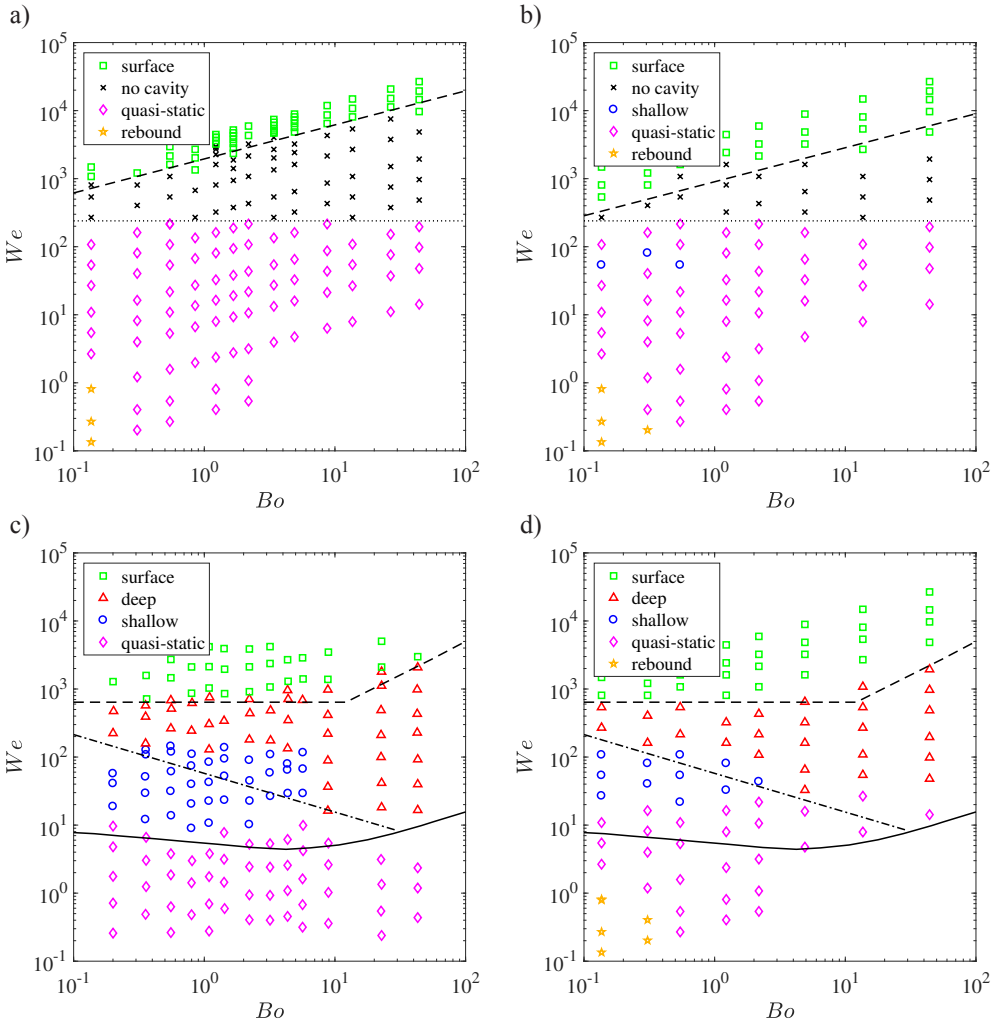

FIGURE 2. The cavity regimes for various contact angles are shown for a) $\theta = 86.1°$, b) $\theta = 101.1°$, c) $\theta = 120°$ and $R_z = 50$ μm (remade from Aristoff & Bush (2009)) and d) $\theta = 141.1°$. All of the spheres are smooth according to Zhao *et al.* (2014) except c) (table 1). The dotted and dashed lines in a) and b) represent *splash formation* and *Duez cavity formation*, respectively. The regime separation lines in c) and d) are not the same as in a) and b). Instead they come from the predictions of Aristoff & Bush (2009). Pictures of the different regimes can be seen in figure 1a-e.

depicted in the literature, the collapse of the crown, also know as dome over, causes a complete seal between the air in the cavity and the atmosphere (see supplementary movie 5). Figure 5 shows an event in which a complete seal does not occur during dome over. At $t = 6.4$ ms the splash crown has domed over and the air cavity behind the sphere begins to pull away from the free surface of the pool. At $t = 8.0 - 9.6$ ms air continues to enter the cavity as evidenced by the small conical structure that forms and connects the top of the cavity to the surface of the pool. The conical structure then collapses radially slightly below the surface providing a complete seal ($t = 11.2$ ms). These partial surface seal events could be caused by an asymmetric dome over of the splash crown, that leaves a small hole or by the formation of the thin-filmed bags observed by Marston *et al.*

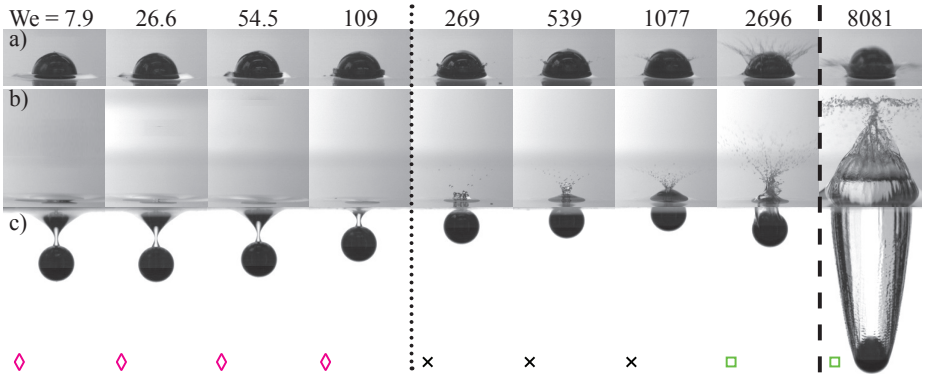

FIGURE 3. The development of the splash and progression of cavity regimes are shown for increasing We, for $d = 10$ mm and $\theta = 101.1°$. Each column shows different times and/or views of the same impact event. In a) we show the development of the rim or splash when the sphere is approximately half submerged. In b) and c) we show the frame just prior to pinch-off or closure of the splash above the sphere as viewed from above and below the pool surface, respectively. The dotted and dashed lines represent *splash formation* and *Duez cavity formation*, respectively, and the symbols indicated the cavity type, which are all shown in figure 2b.

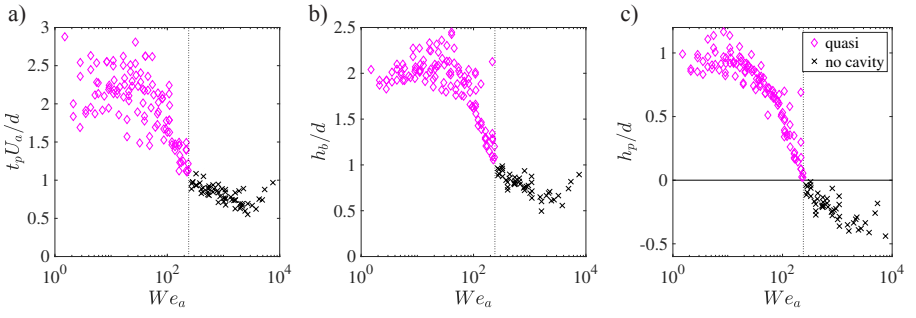

FIGURE 4. a) The non-dimensional pinch-off time t_p, depth of the bottom of the sphere at pinch-off h_b (inset) and b) the pinch-off depth h_p scale with We_a for the quasi-static and no cavity regimes for $\theta = 86.1°$ and $101.0°$. Figure 3c shows the same trends for h_b and h_p qualitatively except that here the surface seal data is not shown as transition occurs at a constant velocity and the data does not collapse with We_a. The dotted line represents the *splash formation line*. Note that the Weber number and dimensionless pinch-off time are defined using the average sphere velocity from initial impact to full submergence U_a ($We_a = \rho U_a^2 d/\sigma$). This accounts for the contiuned acceleration of the sphere when it has not reached the terminal velocity in water by the time it impacts (e.g., an 18 mm sphere falling 3 mm). The legend in b) applies to all three plots.

(2016) that pop leaving holes in the crown. Partial surface seal occurs most commonly just above the critical velocity for cavity formation and at lower contact angles.

At the highest contact angle tested, when $\theta = 141.1°$ Duez *et al.* (2007) predict that cavities should form above a critical velocity of $U_{cr} = \frac{7}{270}\frac{\sigma}{\mu}(\pi - \theta)^3 = 0.58$ m/s. This velocity gives $We < 240$ for all sphere diameters tested. Hence, the *Duez cavity formation* line lies below the *splash formation* line at all Bo tested and we would expect cavities to form at all impact velocities. This is indeed the case as shown in figure 2d. Comparing figure 2d to the data obtained by Aristoff & Bush (2009) for rough spheres with $\theta = 120°$ (shown in figure 2c) we see that the regime locations for the two coatings are very similar. Discrepancies in the cut off between quasi-static seal and shallow or deep seal are possibly due to the lower atmospheric pressure in Logan, Utah (elevation of 1382 m) where our

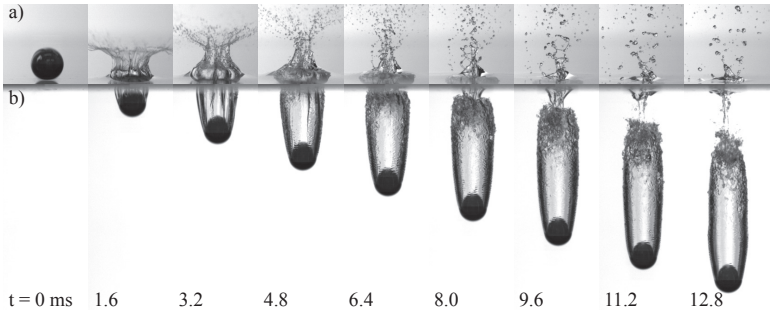

FIGURE 5. A sphere with $d = 10$ mm and $\theta = 101.1°$ impacts the pool surface at $U = 6.26$ m/s forming a surface seal cavity with the above and below water views shown in a) and b) respectively. The splash crown does not always provide a complete seal of the cavity during dome over. Sometimes it mostly seals, but allows some air continue to enter the cavity as shown by the conical air pocket near the surface and above the main portion of the cavity at $t = 9.6$ ms. The conical portion of the cavity then collapses radially ($t = 11.2 - 12.8$ ms). See supplementary movie 6.

experiments were performed and Cambridge, Massachusetts (elevation of 40 m) where the experiments of Aristoff & Bush (2009) were performed, with the lower pressure leading to less air entrainment as shown by Gilbarg & Anderson (1948), persisting for larger We. Discrepancies could also be due to the difference in roughness or the difference in wetting angle, or all three effects combined.

Spheres rebound off of the pool surface at the lowest Bo and We tested for all three contact angles. Figure 2 shows that transition from water entry to rebound occurs when $We = 1$ and $Bo < 1$. In this parameter space surface tension dominates over both inertial and gravitational forces and hence, neither the sphere's inertia nor its weight cause it to enter the water surface. Figure 2 also shows that rebound is slightly dependent on the sphere's contact angle, with higher contact angles leading to rebound at higher Bo and We.

4. A new scaling

When defining dimensionless numbers it is always difficult to pick the appropriate length and velocity scales to describe the physics of the problem. Historically in water entry research, the sphere diameter or radius has been chosen as the length scale and the initial impact velocity for the velocity scale (Truscott *et al.* 2014). As the cavity collapse is likely to be a function of the cavity characteristics, it could be insightful to redefine the appropriate dimensionless numbers using cavity length and velocity scales. We define the cavity Weber number as $We_c = \rho U_c^2 d_c/\sigma$, the cavity Bond number as $Bo_c = \rho g d_c^2/\sigma$ and the cavity Froude number as $Fr_c = U_c^2/g d_c$, where d_c is the cavity diameter defined in §2 and U_c is the downward cavity velocity, which we set equal to the initial sphere impact velocity U_o as they are approximately the same. Plotting a regime diagram with the cavity scaling for $\theta = 141.1°$, we see in figure 6 that Bo_c and We_c separate the cavity types for shallow, deep and surface seal (hollow symbols). Quasi-static seal cavities are not included because they are not cylindrical and they are specific to sphere entry as discussed more in the next paragraph.

Speirs *et al.* (2018) investigated the water entry of multi-droplet streams and jets and found that shallow, deep and surface seal cavities occur for liquid-liquid impact as well. In that paper we predicted the cavity seal types for both multi-droplet streams and jets on the same Bo-We regime diagram using a scaling based on the cavity diameter and no

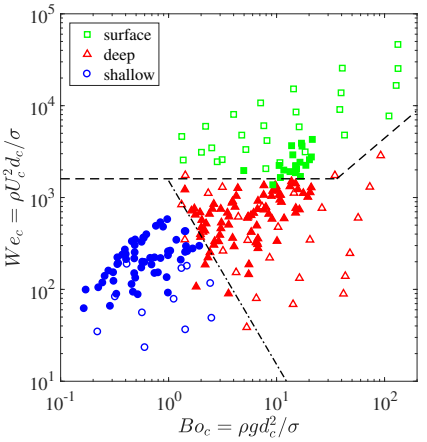

FIGURE 6. The cavity regimes can be predicted for various impacting bodies using the cavity diameter d_c and cavity velocity U_c to define Bo_c and We_c. The hollow symbols are for spheres and the solid symbols are for multi-droplet streams and jets. The dash-dotted line separating the shallow and deep seal regimes is found by equating the dimensionless pinch-off times for shallow and deep seal (figure 7). The dashed line dividing deep and surface seal is drawn by modifying the cutoffs found by Aristoff & Bush (2009) and Birkhoff & Isaacs (1951).

alteration of the impact velocity. We can collapse those data onto the Bo_c-We_c regime diagram for spheres using d_c and U_c to define Bo_c and We_c as in figure 6. The cavity velocity U_c is set equal to one half the impacting stream velocity for simplicity, which is shown to be a good approximation for jets in Speirs *et al.* (2018). Using this scaling, figure 6 shows that the regimes for all three water entry types (spheres, liquid jets and liquid multi-droplet streams) can be predicted in the same Bo_c-We_c parameter space. This scaling suggests that we can predict the pinch-off type of a cavity if we know its diameter and downward velocity, regardless of the type of impacting body used.

The cavity nondimensional pinch-off times, $t_p U_c/d_c$, of the sphere, multi-droplet stream and jet data can be predicted on the same plot for shallow and deep seal using We_c and Fr_c, respectively. Figure 7a shows that $t_p U_c/d_c$ scales with $We_c^{1/2}$ for shallow seal and figure 7b shows that $t_p U_c/d_c$ scales with $Fr_c^{1/3}$ for deep seal. Equating these nondimensional pinch-off times and rearranging gives the cut-off between the shallow and deep seal regimes as shown by the dash-dotted line in figure 6 ($We_c = 1,525 Bo_c^{-2}$).

To predict the cut-off for surface seal we look at previous works. Aristoff & Bush (2009) used an empirical fit of $We = 640$ to define the cut-off for surface seal at low Bo while at high Bo Birkhoff & Isaacs (1951) predicted the cut-off to occur at $Fr = 1/12800(\rho/\rho_a)^2$, where ρ_a is the air density. We can use these results to find the surface seal cut-off in terms of We_c and Fr_c. At low Bo_c, the cut-off is $We_c = 640(d_c/d)_{mean}$, where $(d_c/d)_{mean} \approx 2.5$ is the mean cavity to sphere diameter ratio for the deep and surface seal data just above and below the transition at low Bo_c. This leads to a transition at $We_c = 1600$. At high Bo_c, the cut-off is $Fr_c = 1/12800(\rho/\rho_a)^2(d/d_c)_{mean}$, where $(d/d_c)_{mean} \approx 1.6$ is the mean for the deep and surface seal data just above and below the transition at high Bo_c. This leads to a transition at $Fr_c = 44$ or $We_c = 44 Bo_c$. These transitional lines are shown in figure 6 with the dashed line and appropriately divide the deep and surface seal regimes. It is interesting to note that the shallow, deep and surface seal transition lines intersect at $Bo_c = 1$, indicating that when surface tension dominates over gravitational forces, shallow seal will always occur instead of deep.

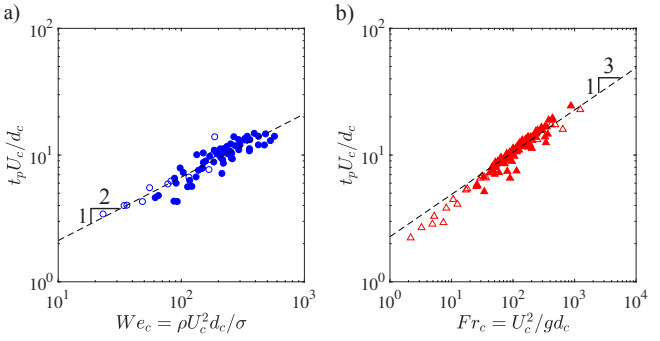

FIGURE 7. The nondimensional cavity pinch-off time scales with We_c and Fr_c for a) shallow and b) deep seal for spheres with contact angle $\theta = 141.1°$ (hollow symbols) and multi-droplet streams and jets (solid symbols). The dashed lines are fits to the data with powers forced to $t_pU_c/d_c = 0.67We_c^{1/2}$ for shallow seal and $t_pU_c/d_c = 2.27Fr_c^{1/3}$ for deep seal.

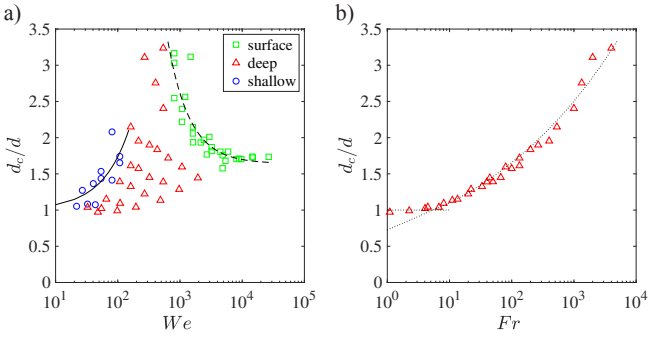

FIGURE 8. The cavity diameter for the impact of spheres with $\theta = 141.1°$ scales with We for shallow and surface seal a) and Fr for deep seal b). The solid and dashed lines in a) are least square regressions with $d_c/d = 0.0074We + 1$ for shallow seal and $d_c/d = 4952We^{-1.24} + 1.64$ for surface seal. The curved dotted line in b) is a fit for the deep seal data ($d_c/d = 0.73Fr^{0.18}$), but for $Fr < 7$ the cavity diameter approaches the sphere diameter, $d_{cav}/d = 1$ marked by the horizontal dotted line.

Seeing the importance of the cavity diameter in calculating Bo_c and We_c, we now scale d_c for each pinch-off type. Plotting the nondimensional cavity diameter d_c/d against We we see in figure 8a that the cavity diameter for the shallow seal data is a function of We and can be predicted with a linear fit of $d_c/d = 0.0074We + 1$, where the y-intercept is forced to equal one sphere diameter. We can also predict the cavity diameter for the surface seal data using We with the fit $d_c/d = 4952We^{-1.24} + 1.64$. As commonly seen, the deep seal data scales better with Fr as shown in figure 8b and can be predicted by $d_c/d = 0.73Fr^{0.18}$ for high Fr, but below $Fr \approx 7$ the ratio d_c/d asymptotes to one.

5. Conclusion

Cavity formation is dependent on the formation and behavior of the splash crown. Three crown behaviors exist. 1) At low We a slow-moving, thick rim forms around the sphere, which allows air to entrain in the wake of the sphere forming small cavities. 2) At higher We the crown thins and gains velocity which allows it to adhere to the sphere, climb the surface, and meet at the apex to preventing cavity formation. 3) Once the critical velocity for cavity formation is reached the splash crown separates from the

sphere forming the classical cavities discussed above and in previous works. The cutoffs between these behaviors are defined by *splash formation* and *Duez cavity formation*. For hydrophilic and slightly hydrophobic spheres, the inception of splash formation and adherence to the sphere decreases the cavity size, compared to higher contact angles, leading to quasi-static seal and small shallow seal cavities. When the contact angle is high enough ($\theta \gtrsim 140°$) or the sphere is rough (Zhao *et al.* 2014), cavities form at all impact velocities because the splash crown either does not form or it separates from the sphere. These cavity formation regimes are predicted by Aristoff & Bush (2009). When cavity formation is not inhibited by the splash, the pinch-off type can be predicted by the cavity diameter and downward cavity velocity regardless of the type of impacting body (e.g., sphere, jet, or multi-droplet stream). This forms a more complete picture, linking the impact of solids and liquids on liquid pools.

6. Acknowledgments

N.B.S., T.T.T. and J.B. acknowledge funding from the Office of Naval Research, Navy Undersea Research Program (grant N0001414WX00811), monitored by Ms. Maria Medeiros. J.B. acknowledges funding from the Naval Undersea Warfare Center In-House Laboratory Independent Research program, monitored by Mr. Neil Dubois. N.B.S and T.T.T acknowledge funding from the Utah State University Research and Graduate Studies Development Grant Program.

REFERENCES

Aristoff, J. M. & Bush, J. W. M. 2009 Water entry of small hydrophobic spheres. *Journal of Fluid Mechanics* **619**, 45–78.

Aristoff, J. M., Truscott, T. T., Techet, A. H. & Bush, J. W. M. 2010 The water entry of decelerating spheres. *Physics of Fluids* **22** (3).

Birkhoff, G. & Isaacs, R. 1951 Transient cavities in air-water entry. Navord Report 1490. Tech. Rep.

Duez, C., Ybert, C., Clanet, C. & Bocquet, L. 2007 Making a splash with water repellency. *Nat Phys* **3** (3), 180–183.

Gilbarg, D. & Anderson, R. A. 1948 Influence of atmospheric pressure on the phenomena accompnaying the entry of spheres into water. *J. Appl. Phys.* **19**, 127–139.

Hurd, R. C., Belden, J., Jandron, M. A., Fanning, D. T., Bower, A. F. & Truscott, T. T. 2017 Water entry of deformable spheres. *Journal of Fluid Mechanics* **824**, 912–930.

Mansoor, M. M., Marston, J. O., Vakarelski, I. U. & Thoroddsen, S. T. 2014 Water entry without surface seal: extended cavity formation. *Journal of Fluid Mechanics* **743**, 295–326.

Marston, J. O., Truscott, T. T., Speirs, N. B., Mansoor, M. M. & Thoroddsen, S. T. 2016 Crown sealing and buckling instability during water entry of spheres. *Journal of Fluid Mechanics* **794**, 506–529.

Speirs, N. B., Pan, Z., Belden, J. & Truscott, T. T. 2018 The water entry of multi-droplet streams and jets. *Journal of Fluid Mechanics* **844**, 1084–1111.

Truscott, T. T., Epps, B. P. & Belden, J. 2014 Water entry of projectiles. *Annual Review of Fluid Mechanics* **46** (1), 355–378.

Truscott, T. T., Epps, B. P. & Techet, A. H. 2012 Unsteady forces on spheres during free-surface water entry. *Journal of Fluid Mechanics* **704**, 173–210.

Truscott, T. T. & Techet, A. H. 2009*a* A spin on cavity formation during water entry of hydrophobic and hydrophilic spheres. *Physics of Fluids* **21** (12), 121703.

Truscott, T. T. & Techet, A. H. 2009*b* Water entry of spinning spheres. *Journal of Fluid Mechanics* **625**, 135–165.

Zhao, M.-H., Chen, X.-P. & Wang, Q. 2014 Wetting failure of hydrophilic surfaces promoted by surface roughness. *Scientific Reports* **4**, 5376.